Miner Deposita (2006) 41: 82–98
DOI 10.1007/s00126-005-0043-5

ARTICLE

Georges Beaudoin · René Therrien · Catherine Savard

3D numerical modelling of fluid flow in the Val-d'Or orogenic gold district: major crustal shear zones drain fluids from overpressured vein fields

Received: 1 January 2005 / Accepted: 6 December 2005 / Published online: 28 February 2006

Abstract Fluid flow patterns have been determined using oxygen isotope isopleths in the Val-d'Or orogenic gold district. 3D numerical modelling of fluid flow and oxygen isotope exchange in the vein field shows that the fluid flow patterns can be reproduced if the lower boundary of the model is permeable, which represents middle or lower crustal rocks that are infiltrated by a metamorphic fluid generated at deeper levels. This boundary condition implies that the major crustal faults so conspicuous in vein fields do not act as the only major channel for upward fluid flow. The upper model boundary is impermeable except along the trace of major crustal faults where fluids are allowed to drain out of the vein field. This upper impermeable boundary condition represents a low-permeability layer in the crust that separates the overpressured fluid from the overlying hydrostatic fluid pressure regime. We propose that the role of major crustal faults in overpressured vein fields, independent of tectonic setting, is to drain hydrothermal fluids out of the vein field along a breach across an impermeable layer higher in the crust and above the vein field. This breach is crucial to allow flow out of the vein field and accumulation of metals in the fractures, and this breach has major implications for exploration for mineral resources. We propose that tectonic events that cause episodic metamorphic dehydration create a short-lived pulse of metamorphic fluid to rise along zones of transient permeability. This results in a fluid wave that propagates upward carrying metals to the mineralized area. Earthquakes along crustal shear zones cause dilation near jogs that draw fluids and deposit metals in an interconnected network of subsidiary shear zones. Fluid flow is arrested by an impermeable barrier separating the hydrostatic and lithostatic fluid pressure regimes. Fluids flow through the evolving and interconnected network of shear zones and by advection through the rock matrix. Episodic breaches in the impermeable barrier along the crustal shear zones allow fluid flow out of the vein field.

Keywords Numerical modelling · Fluid flow · Stable isotopes · Crustal shear zones · Gold · Silver · Zinc · Lead

Editorial handling: R. Goldfarb

G. Beaudoin (✉) · R. Therrien · C. Savard
Département de géologie et de génie géologique,
Université Laval,
Québec, QC, G1K 7P4, Canada
e-mail: beaudoin@ggl.ulaval.ca

Introduction

Large crustal faults are commonly considered to have been major channels that controlled flow of deep-seated hydrothermal fluids towards higher crustal levels to form mineral deposits in vein fields (Beaudoin et al. 1992b; Groves 1993; Groves et al. 2003; Hagemann and Cassidy 2000; Sibson et al. 1988; Kerrich et al. 1987; Goldfarb et al. 2001). That interpretation is based mainly on the occurrence of veins nearby and along the trace of major crustal fault zones, as shown in Fig. 1 for the Superior province, Canada. Elegant and convincing models have been proposed to explain the structural setting of the veins (Robert and Brown 1986; Sibson et al. 1988; Robert et al. 1995; Boullier and Robert 1992; Cox and Ruming 2004), but the relationship between gold mineralization and the major crustal faults remains a paradox as these major fault zones are devoid of significant gold mineralization. This observation is contrary to what might be expected if these faults were major fluid conduits for hydrothermal fluids as suggested by many authors (Eisenlohr et al. 1989; Kerrich and Ludden 2000; Groves et al. 1998; Hagemann and Cassidy 2000; Cox et al. 2001; Kerrich and Wyman 1990; Kerrich et al. 1987; Neumayr and Hagemann 2002).

Along the trace of major crustal shear zones, vein fields tend to form where the shear is at high angle to the regional trend (Weinberg et al. 2004). Stress transfer modelling for the Mount Pleasant and St. Ives districts, Yilgarn Craton, Australia, indicates that the vein fields formed in areas adjacent to the major shear where aftershocks created transient permeability near dilatant or contractional jogs that arrest rupture propagation (Micklethwaite and Cox 2004; Cox and Ruming 2004). In the Val-d'Or vein field,

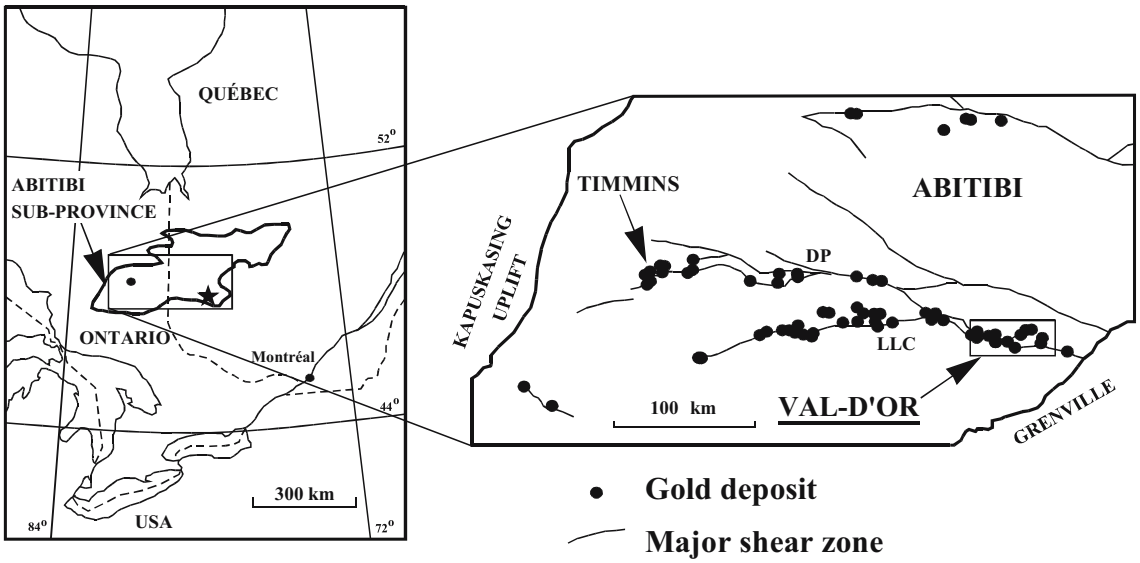

Fig. 1 Distribution of gold deposits in the Abitibi sub-province, Canada. The deposits occur along the trace of major crustal shear zones such as the Larder Lake-Cadillac (*LLC*) and the Destor-Porcupine (*PD*) shear zones. Deposits form clusters (vein fields) separated by gaps where no major gold deposit is known. The Val-d'Or vein field is shown in detail in Fig. 2 (modified from Robert and Kelly 1987; Robert et al. 1995)

for example, a few veins are in the Cadillac tectonic zone, but most are in subsidiary shear zones up to 15 km north of the Cadillac tectonic zone (Fig. 2), and yet fluid inclusions indicate essentially the same type of fluids in the Cadillac tectonic zone as elsewhere in the vein field (Neumayr and Hagemann 2002; Neumayr et al. 2000; Robert 1994). This long-held intuitive concept is examined here in an innovative approach combining 3D numerical modelling of fluid flow and oxygen isotope exchange between hydrothermal fluids and a porous rock matrix cut by high-permeability zones (Beaudoin and Therrien 1999). The genetic relationship between the major crustal shear zones and the precious and base metal vein fields is an important concept to understand, both for scientific understanding of crustal-scale fluid flow and for practical aspects of mineral exploration.

Mapping fluid flow patterns in vein fields

Vein fields are domains of the crust that were fractured and sealed by hydrothermal minerals, and, as such, they represent fossilized crustal-scale hydrothermal systems. Vein fields can be recognized by the occurrence of an abnormally high abundance of veins (100 s to 1,000 s) in a segment of crustal rocks. These fractured domains represent openings during fluid pressure build-up before and during aftershock slip following major earthquakes (Boullier and Robert 1992; Micklethwaite and Cox 2004; Cox and Ruming 2004). To form a vein field, the veins must display a consistent mineralogical assemblage and must have formed in a dominant mechanical and stress regime during a defined period. These characteristics render vein fields attractive to study crustal-scale hydro-

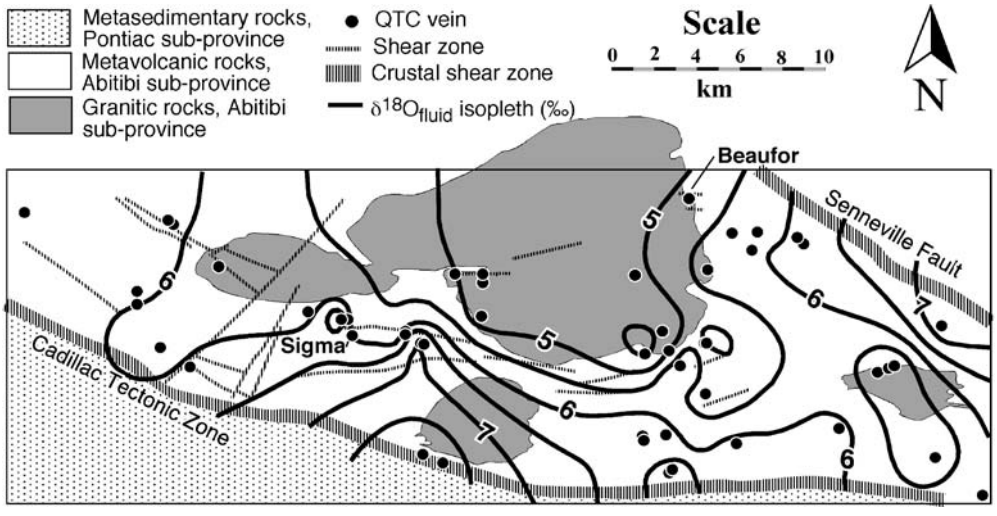

Fig. 2 Val-d'Or vein field oxygen isotope composition of hydrothermal fluids, calculated at 350°C, from quartz–tourmaline–carbonate (*QTC*) vein $\delta^{18}O_{quartz}$ values (Beaudoin and Pitre 2005). Fluid oxygen isotopleths are contoured from a regular grid obtained by krieging average deposit $\delta^{18}O_{quartz}$ values (Beaudoin and Pitre 2005) within the rectangular surface of the 3D domain modelled numerically

thermal systems. In addition, most vein fields contain significant precious (Au–Ag) and base (Ag–Pb–Zn) metal accumulations such that understanding the physical and chemical processes that lead to their formation has important consequences for mineral exploration. The minerals precipitated in the fractures of an active vein field record the chemical composition and physical conditions during fluid flow and precipitation. The oxygen isotope composition of vein minerals is one of the most powerful tools to decipher the fluid composition, source and the water–rock reaction history of the hydrothermal system because oxygen is the most abundant element in the fluid and mineral phases.

The Val-d'Or orogenic gold vein field

The Val-d'Or orogenic gold formed in two events during regional compression, before and after about 2,692 Ma based on cross-cutting relations with dykes (Couture et al. 1994; Robert 1994). The second event formed the quartz–tourmaline–carbonate vein field after peak metamorphism (Hanes et al. 1992). The quartz–tourmaline–carbonate vein field is in subsidiary structures to the Cadillac tectonic zone, a major terrane boundary between the Pontiac and Abitibi Archean sub-provinces (Fig. 2). Because isotope equilibrium temperatures display no gradient, and because the range in equilibrium temperatures is comparable to uncertainty of the geothermometers and to the range in fluid inclusion temperatures in the vein field, it can be assumed that the vein field was under broadly isothermal conditions (Beaudoin and Pitre 2005; Pitre 2000). If oxygen isotope compositions were controlled by a temperature gradient, one would expect that carbon and sulphur isotope systems would also behave accordingly, which is not the case in the Val-d'Or vein field (Beaudoin and Pitre 2005; Pitre 2000). The absence of a strong temperature gradient distinguishes overpressured vein fields from epithermal veins and other hydrothermal systems under hydrostatic fluid pressure that commonly display strong temperature gradients.

Using the isothermal condition assumption and the most likely temperature for isotope equilibrium of 350°C, $\delta^{18}O_{fluid}$ values (Fig. 2) can be calculated from the quartz–tourmaline–carbonate veins (Beaudoin and Pitre 2005; Pitre 2000). Oxygen isotope composition in quartz–tourmaline–carbonate veins displays a regional zonation (Fig. 2) that is interpreted to result from mixing of a deep-seated metamorphic fluid, infiltrating from below and with a minimum $\delta^{18}O$ value of 8.5‰, with a supracrustal fluid with a maximum $\delta^{18}O$ value of 3.9‰ that had a long history of water–rock oxygen exchange (Beaudoin and Pitre 2005; Pitre 2000). The Val-d'Or vein field displays high $\delta^{18}O_{fluid}$ values, above 7.5‰, north of the Cadillac tectonic zone in the south-central part of the vein field. The $\delta^{18}O_{fluid}$ decreases from the south-central part towards the north and cuts across all lithological and structural contacts (Beaudoin and Pitre 2005). A SE–NW valley of lower $\delta^{18}O_{fluid}$ values in the southeast corner of the vein field is followed by higher $\delta^{18}O_{fluid}$ values towards the northeast corner of the vein field, along the trace of the Senneville shear zone (Fig. 2). This regional $\delta^{18}O_{fluid}$ isopleth pattern is thought to map auriferous fluid flow and reaction in the vein field.

Numerical model

The 3D variably saturated flow and solute transport model presented by Therrien and Sudicky (1996) has been modified to simulate fluid flow and oxygen isotope transport and reaction in fractured geologic materials. The discrete fracture conceptual model is adopted, where fluid flow and solute transport are simulated in 2D discrete fractures located in a 3D porous rock matrix, which is permeable. Governing equations for flow and solute transport are thus required for both the 2D discrete fractures and the 3D porous matrix. This section presents these equations and the numerical methods used to solve them. Compared to the study presented by Therrien and Sudicky (1996), it is assumed here that both fractures and porous matrix are fully saturated, and the variably saturated options of the original model are not used.

The equation for 3D fluid flow in a saturated porous medium is:

$$\frac{\partial}{\partial x_i}\left(K_{ij}\frac{\partial h}{\partial x_j}\right) \pm Q = S_s\frac{\partial h}{\partial t} \quad i,j = 1,2,3 \tag{1}$$

where K_{ij} is the porous medium hydraulic conductivity tensor [$L\,T^{-1}$], h is hydraulic head [L], Q is the volumetric fluid flux per unit volume representing a source or sink to the porous medium [$L^3\,L^{-3}\,T^{-1}$] and S_s is the specific storage coefficient of the porous medium [L^{-1}].

2D fluid flow in a discrete fracture of aperture $2b$ [L] is described by:

$$\frac{\partial}{\partial x_i}\left(2b\,K_f\frac{\partial h_f}{\partial x_j}\right) - q_{n/I^-} + q_{n/I^+} \pm Q_f = 2b\,S_{sf}\frac{\partial h_f}{\partial t} \quad i,j = 1,2 \tag{2}$$

where h_f and K_f are the hydraulic head [L] and hydraulic conductivity of the fracture, respectively, Q_f is the volumetric fluid flux per unit area representing a source or sink (+ or − sign, respectively) to the fracture [$L^3\,L^{-2}\,T^{-1}$] and S_{sf} is the specific storage coefficient of the fracture [L^{-1}]. In Eq. (2), fluid exchange between the fracture and the matrix is represented by leakage fluxes terms $q_{n|I^-}$ and $q_{n|I^+}$ [$L^3\,L^{-2}\,T^{-1}$) that are normal to the surfaces I^- and I^+ of a fracture. The assumption is made here that the hydraulic head in the matrix along those surfaces is equal to the hydraulic head in the fractures.

The hydraulic conductivity of a fracture is generally assumed to be a function of its aperture, such that:

$$K_f = \frac{\rho g (2b)^2}{12\mu} \tag{3}$$

where ρ and μ are the fluid density [M L^{-3}] and viscosity [M L^{-1} T^{-1}], respectively, and g is the acceleration due to gravity [L T^{-2}]. In the model, high-permeability planes can be represented by Eq. (2), in which case $2b$ corresponds to the thickness of the plane and K_f is its hydraulic conductivity, which is not assumed to be a function of the thickness and thus not computed with Eq. (3).

Therrien and Sudicky (1996) presented an equation describing 3D advective–dispersive transport of a dissolved solute in a porous medium. That equation has been modified to simulate partitioning of oxygen isotope between rock and water using the formulation presented by Bowman et al. (1994):

$$\frac{\partial}{\partial x_i}\left(D_{ij}\frac{\partial R_w}{\partial x_j}\right) - \frac{q_i}{n}\frac{\partial R_w}{\partial x_i} = \frac{\partial}{\partial t}\left(R_w + \frac{X_k}{X_w}R_k\right) \quad i,j = 1,2,3 \tag{4}$$

where q_i is the volumetric fluid flux [L T^{-1}] obtained from Darcy's law and n is the porosity of the porous medium [L^3 L^{-3}]. The mass fractions of oxygen in the rock and the fluid per unit volume of fluid saturated porous medium are given by X_k and X_w, respectively. The hydrodynamic dispersion tensor of the porous medium D_{ij} [L^2 T^{-1}] is given by:

$$nD_{ij} = \left(\alpha_l - \alpha_t D_{ij}\right)\frac{q_i q_j}{|q|} + \alpha_t |q|\delta_{ij} + n\tau^* D_o \delta_{ij} \quad i,j = 1,2,3 \tag{5}$$

where α_l [L] and α_t [L] are the longitudinal and transverse dispersivity of the porous medium, respectively, δ_{ij} is the dimensionless Kronecker delta function defined such that δ_{ij}=1 for i=j and δ_{ij}=0 otherwise, τ* is the dimensionless tortuosity of the porous matrix and D_o [L^2 T^{-1}] is the free-solution diffusion coefficient for the solute. The hydrodynamic dispersion tensor accounts for the effect of mechanical dispersion, given by the first two terms on the right-hand side of Eq. (5), and molecular diffusion, which is the last term on the right-hand side of Eq. (5). Mechanical dispersion is defined as the spreading of a solute caused by small-scale fluid flux variations about the mean value q_i (Domenico and Schwartz 1998).

The $^{18}O/^{16}O$ of the fluid and the rock are given by R_w and R_k, respectively, and they are treated as concentrations in the model, an approximation that is valid for oxygen isotopes (Criss et al. 1987). Oxygen partitioning between the fluid and the solid phase is assumed to follow a first-order rate reaction (Criss et al. 1987) such that:

$$\frac{\partial R_k}{\partial t} = k_k(\alpha_k R_w - R_k) \tag{6}$$

where k_k is the reaction rate of the controlling surface reaction [T^{-1}] and α_k is the oxygen isotope fractionation factor between water and the rock matrix.

Equations (4) and (6) indicate that the evolution of the $^{18}O/^{16}O$ ratio during water/rock reaction is controlled by several parameters including the rate of fluid infiltration, diffusive and dispersive properties of the porous rock matrix, rate of isotope exchange, rock/water mass oxygen ratio and water/mineral fractionation. Temperature also affects the evolution of the $^{18}O/^{16}O$ ratio, but isothermal conditions are assumed here.

It is currently assumed in the model that oxygen partitioning between the fluid and solid phase occurs only in the 3D porous matrix, and it is not accounted for in the 2D fracture. As a result, the equation governing oxygen transport in a 2D fracture can be written as:

$$2b\left[\frac{\partial}{\partial x_i}\left(D_{fij}\frac{\partial R_w}{\partial x_j}\right) - q_{fi}\frac{\partial R_w}{\partial x_i}\right] + \Omega_{n/I^+} - \Omega_{n/I^-} = 2b\frac{\partial R_w}{\partial t} \quad i,j = 1,2 \tag{7}$$

where D_{fij} is the hydrodynamic dispersion tensor of the fracture [L^2 T^{-1}] defined in a manner similar to Eq. (5) for the porous matrix, and q_{fi} is its volumetric fluid flux in the fracture obtained from Darcy's law [L T^{-1}]. The terms involving Ω_n represent normal advective and dispersive mass fluxes across the fracture surfaces. Similar to the flow equation, it is assumed that the concentration in the matrix at the fracture surfaces is equal to that in the matrix.

The model uses the control volume finite element technique to discretize flow Eqs. (1) and (2) as well as transport Eqs. (4) and (7), which ensures local and global mass conservation. The porous medium is discretized in three dimensions, and 2D elements are used to represent fractures. Nodes attached to the fracture elements are coincident with those belonging to adjacent porous medium elements. Following discretization, the matrix contributions arising from the discretization of the fractures are superimposed onto those stemming from the discrete form of the equation for the porous medium. Continuity in hydraulic head and concentration is therefore ensured at the fracture/porous media interface, and this coupling method thus avoids the need for a direct evaluation of the exchanges fluxes q_n and Ω_n between the fracture and the porous medium elements. The resulting system of equations is solved with a preconditioned iterative matrix solver. More

details on the numerical solution of the governing equations are presented in Therrien and Sudicky (1996).

Model verification

The numerical model has been verified by reproducing known results for 3D fluid flow and solute transport in discretely fractured media (Therrien and Sudicky 1996). This section presents additional verification of the model for simulating reactive transport of oxygen isotopes. The model is compared to a 1D analytical solution to the oxygen transport and reaction equations that solved nondimensional forms of Eqs. (4) and (6) (Bowman et al. 1994). Although Eqs. (4) and (6) are in dimensional form, direct comparison to simulation results presented by Bowman et al. (1994) is possible by selecting input parameters for Eqs. (4) and (6) that produce values for nondimensional parameters similar to those used by Bowman et al. (1994). Results for this comparison use the definitions given by Bowman et al. (1994) for nondimensional time τ:

$$\tau = \frac{qt}{nL} \tag{8}$$

where t is the time [T] and L is the total length of the 1D domain, as well as nondimensional distance Z:

$$Z = \frac{z}{L} \tag{9}$$

where z is the distance [L] taken from the origin of the porous medium.

The verification of the example presented by Bowman et al. (1994) is for 1D oxygen transport and kinetically controlled isotopic exchange where the dimensionless distance Z is equal to 1. The Peclet and Damkohler numbers, used by Bowman et al. (1994) in that example, are equal to 100 and 0.1, respectively. To simulate this problem, a 3D finite element grid having dimensions of 1 m in each of the X-, Y- and Z-directions is generated using rectangular block elements. A uniform nodal spacing equal to 1 m in the X- and Y-directions and 0.02 m in the Z-direction is chosen, such that a single element discretizes the domain in the X- and Y-directions. This discretization effectively makes the problem 1D with flow and transport in the Z-direction only and allows direct comparison to the simulations presented by Bowman et al. (1994).

The boundary conditions and the material properties of the porous matrix are arbitrarily chosen such that the Peclet and Damkohler numbers mentioned above apply for the simulation. The matrix has a hydraulic conductivity and porosity equal to 0.1 m year^{-1} and 0.01, and its longitudinal dispersivity is equal to 0.01 m. Molecular diffusion is assumed negligible for the simulation. The rock–water mass ratio is equal to 0.02, the fractionation factor is 1.0053 and the reverse reaction rate is equal to 0.1. Steady-state fluid flow is simulated, with prescribed hydraulic heads equal to 0.01 m and 0.0 m at Z=0.0 m and Z=1.0, respectively. For transport, the initial $^{18}O/^{16}O$ of the fluid and the rock are 0.0020054 and 0.002017432, respectively, corresponding to $\delta^{18}O$ values of 0 and 6‰, respectively. A value of $^{18}O/^{16}O$ equal to 0.001985346 ($\delta^{18}O$=−10‰) is imposed at the inflow boundary (Z=0 m) at the start of the simulation and maintained for the total simulation time equal to 8 years. Comparison of the simulated $\delta^{18}O$ of the fluid to that computed by Bowman et al. (1994) is shown in Fig. 3 for different dimensionless time values, illustrating the migration of the fluid having lower $\delta^{18}O$ in the simulation domain. The agreement between the two sets of results provides confidence that our model correctly solves Eqs. (4) and (6).

Illustrative examples

This section presents results of simulations that show the influence of discrete fractures on oxygen isotope patterns for a simplified geological situation. The simulation domain has dimensions of 1 m×1 m×1 m and is discretized with cubic elements having uniform dimensions equal to 0.033 m in each of the X-, Y- and Z-directions, resulting in a total of 27,000 elements and 29,791 nodes for the 3D domain. The porous medium is assumed homogeneous with material properties typical of massive, fresh igneous rocks (Table 1).

For all simulations, steady-state fluid flow is simulated by imposing hydraulic heads at the inflow boundary located at X=0 m and at the outflow boundary located at the X=1 m, such that flow is along the positive X-direction. All other boundaries of the domain are assumed impermeable. The initial $\delta^{18}O$ values for the fluid and rock in the domain are equal to 0 and 6‰, respectively. To represent a source of hydrothermal fluid, a fluid with a constant $\delta^{18}O$ equal to −10‰ is imposed at the inflow boundary, at X=0.0 m, for the duration of the simulation equal to 300 years. Various fracture configurations are tested. For each case, fractures are represented in the model as high-permeability planes of constant thickness ($2b$) and are discretized with 2D rectangular elements (Table 1).

A first case is presented where a single horizontal fracture, located at Z=0.5 m, extends across the whole domain in the X-direction, from X=0 m to X=1 m, but only from Y=0.3 m to Y=0.7 m in the Y-direction. The fracture is connected to both the inflow and outflow boundaries. Velocities in the fracture are several orders of magnitude larger than those in the rock matrix because of the strong conductivity contrast. The resulting $\delta^{18}O$ distribution in the fluid after 10 years indicates preferential migration along the fracture in the direction of flow, with more limited migration of the invading fluid in the matrix as shown by higher $\delta^{18}O$ values (Fig. 4a). Migration in the fracture is controlled mainly by advection, while diffusion, which is a much slower process, controls $\delta^{18}O$ in the low-permeability rock matrix.

The second case is for a single horizontal fracture similar to the fracture in Fig. 4a, but extending from 0.066 to 1.0 m in the X-direction. Because this fracture does not extend

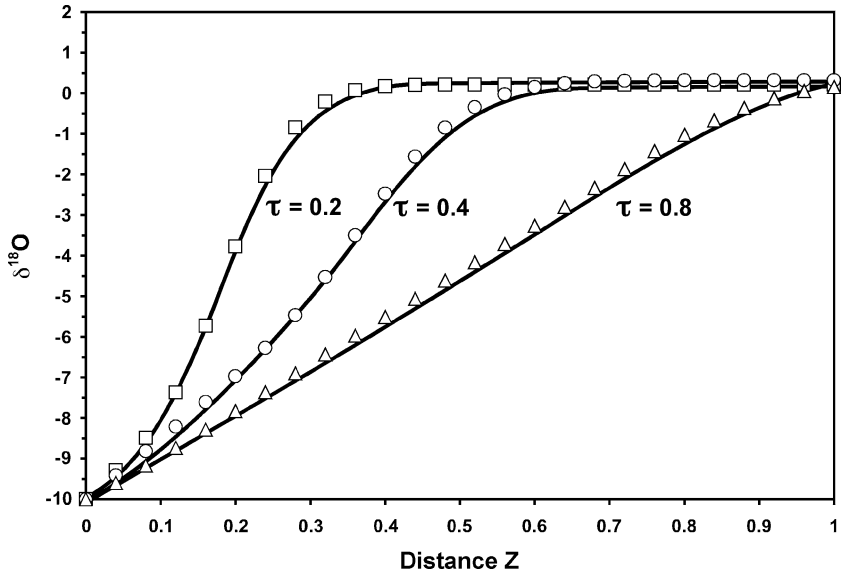

Fig. 3 Fluid $\delta^{18}O$ values along nondimensional distance (Z) at nondimensional time (τ=0.2, 0.4 and 0.8) for kinetic isotope exchange with a Peclet number of 100 and a Damkholer number of 0.1. Initial $\delta^{18}O$ values are interstitial fluid 0‰, infiltrating fluid −10‰, rock matrix +6‰. *Symbols* are results from the numerical model, and *solid lines* are results of Bowman et al. (1994)

across the whole domain in the X-direction, which is the direction of flow generated by the boundary conditions, the hydraulic gradient in the domain is not uniform as shown by the unequal spacing of steady-state hydraulic heads (Fig. 4b). The resulting distribution of oxygen isotopes in the fluid after 300 years of infiltration is shown in Fig. 4c. Because the inflow boundary is not connected to the fracture, the fluid must first migrate through the low-permeability rock matrix, where fluid velocities are very small. Once it reaches the fracture, at X=0.066 m, the invading fluid preferentially migrates along the horizontal fracture, with slower migration in the matrix as indicated by weaker variations in the initial $\delta^{18}O$ outside of the fracture, for Y<0.3 m and Y>0.7 m (Fig. 4c).

A third case has been simulated for a horizontal fracture that is connected to the inflow boundary at X=0 m, but that terminates at X=0.7 m, before reaching the outflow boundary. The $\delta^{18}O$ isopleths simulated after 10 years (Fig. 4d) indicate that the oxygen isotope front has migrated along the plane axis, with little migration of the invading fluid past the end position of the planes, for X>0.7 m. Transport in the matrix is controlled by diffusion, which is reflected by the concentric isopleth distribution around the tip of the fracture (Fig. 4d).

The first three simulations indicate the potential impact of fracture network connectivity on the $\delta^{18}O$ isopleths. The second and third cases can be representative of networks that are not well connected, with dead-end fractures, as opposed to the first case where the fracture is well-connected to the flow system. The configuration of the fracture network will greatly influence spreading of oxygen isotopes since there is much faster solute migration along fractures compared to slow diffusion into the low-permeability matrix.

Another fracture configuration has been explored, where the continuous horizontal fracture of the first case (Fig. 4a) is intersected by a fracture inclined at 45° in the XZ plane (Fig. 4e). The inclined fracture also extends from the inflow to the outflow boundary. The resulting oxygen isotope isopleths, after 5 years, show that the invading fluid preferentially migrates along both fractures, with faster migration along the horizontal fracture (Fig. 4e). Fluid oxygen isotope isopleths in the matrix in the acute angle of fracture intersection show a pattern with convex isopleths upstream and concave isopleths downstream of fluid flow (Fig. 4e). Along the bisector of the acute angle of fracture intersection (Fig. 4f), fluid $\delta^{18}O$ values are initially that of the infiltrating fluid (−10‰) and increase to a $\delta^{18}O$ value of −1.2‰, at X=36 cm, across a sharp front controlled by diffusion in the matrix. After this point, fluid $\delta^{18}O$ values

Table 1 Materials and fluid properties

Property	Value	Unit	Symbol
Saturated porous matrix			
Hydraulic conductivity	10^{-6}	m year^{-1}	K
Porosity	0.018		n
Tortuosity	0.01		τ*
Hydraulic gradient	1.0		
Dispersivity	0.1	m	$\alpha_{l,t}$
Fluid			
Free-solution diffusion coefficient	0.063	m^2 year^{-1}	D_o
Initial composition of porous matrix	+6	‰	
Initial composition of interstitial fluid	0	‰	
Composition of infiltrating fluid	−10	‰	
High-permeability planes			
Hydraulic conductivity	10^{-4}	m year^{-1}	K
Dispersivity	1.0	m	$\alpha_{l,t}$
Thickness	10^{-4}	m	$2b$
Isotope exchange			
Oxygen rock–water mass ratio	122		X_k/X_w
Fractionation factor	1.0053		α_k
Reverse rate of reaction	10^{-5}	year^{-1}	k_k

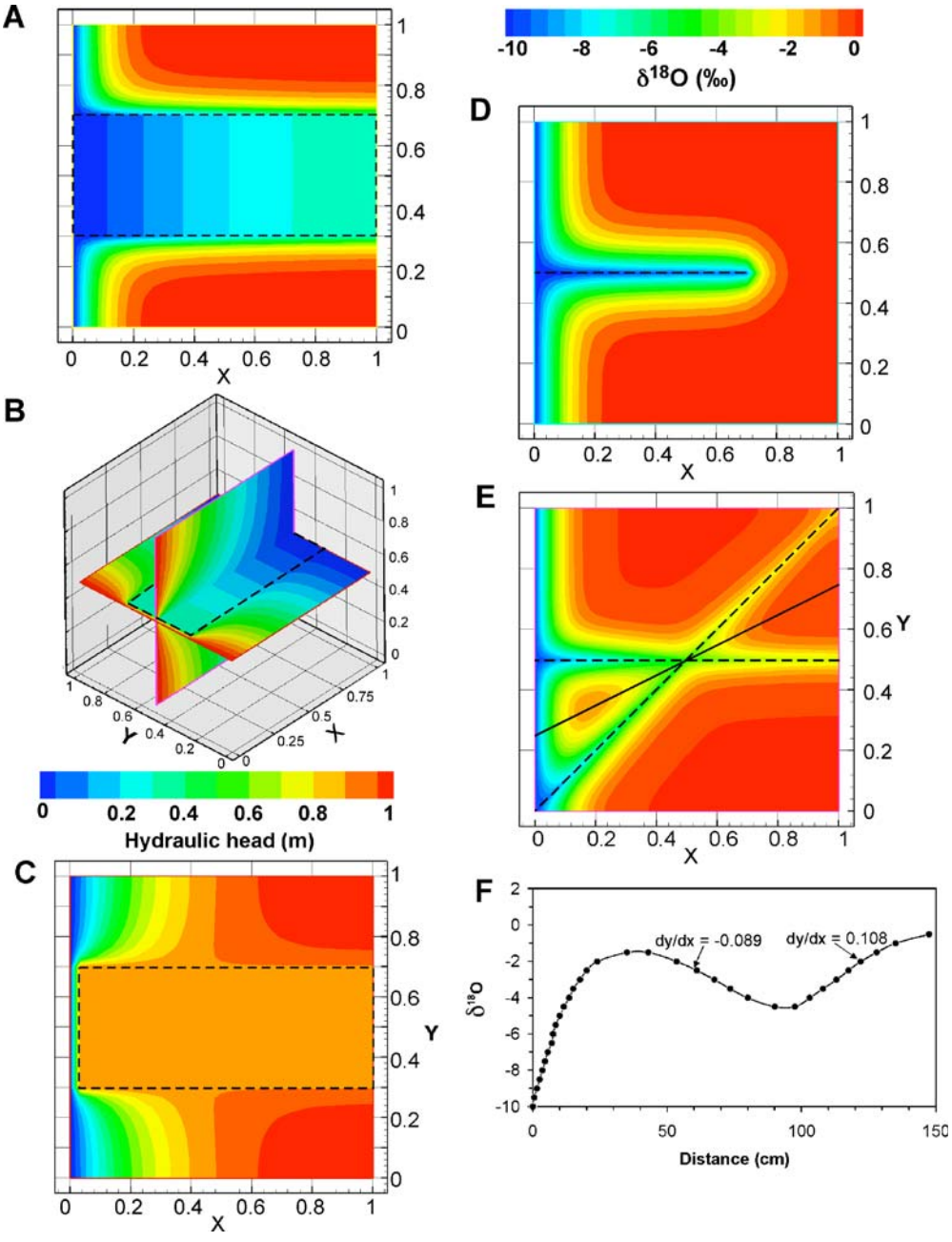

Fig. 4 **a** Fluid oxygen isotope isopleths at t=10 years for a horizontal plane located at Z=0.5 m, corresponding to the plane of a horizontal fracture (*outlined by dashed line*) that extends across the whole domain in the X-direction and is located between Y=0.3 and Y=0.7 m. **b** Steady-state hydraulic head distribution along a vertical plane located at Y=0.5 m and a horizontal plane located at Z=0.5 m, for the case of a horizontal fracture extending from Y=0.3 and Y=0.7 m and from X=0.066 and X=1.0 m (*outlined by dashed line*). **c** Fluid oxygen isotope isopleths at t=300 years for the horizontal plane located at Z=0.5 m for the fracture configuration (*outlined by dashed line*) of **b**. **d** Fluid oxygen isotope isopleths at t=10 years for a vertical cross-section located at Y=0.5 m, for the case of a horizontal fracture (*dashed line*) that extends from X=0.0 to X=0.7 m. **e** Fluid oxygen isotope isopleths at t=5 years for a vertical cross-section located at Y=0.5 m, for the case of a horizontal fracture located at Z=0.5 m that is cut by a fracture inclined at 45° in the XZ plane, extending from X=0.0 and Z=0.0 m to X=1.0 and Z=1.0 m (*dashed lines*) and continuous along the Y-direction. *Black line* marks the fracture intersection acute angle bisector. **f** Fluid δ^{18}O values along the fracture intersection acute angle bisector (X-axis) highlighted in **e**. The derivative (dx/dy) yields the slope at the inflexion points

decrease because of diffusion of fluid from the margins of the fractures until the profile reaches the intersection of the fractures at X=90 cm where the fluid δ^{18}O value is −4.3‰ (Fig. 4f). From this point, fluid δ^{18}O values increase to −0.5‰ as a result of diffusion from the fracture margins (Fig. 4f). An interesting feature of the profile of fluid δ^{18}O values is that the slope (−0.089 at X=60 cm) at the inflexion point on the upstream side of the fracture intersection (X=90 cm) is less steep than the slope (0.108 at X=122 cm) downstream (Fig. 4f), such that anisotropy of isopleth patterns can provide insight into the direction of fluid flow.

3D modelling of fluid flow and reaction in the Val-d'Or vein field

The region of interest in the Val-d'Or area covers the extent of the quartz–tourmaline–carbonate vein field (Fig. 5a) for which the fluid oxygen isotope isopleths (Fig. 2) map the fluid flow and reaction history (Robert 1994; Pitre 2000; Beaudoin and Pitre 2005). The volume of crustal rocks modelled forms a parallelogram that is 45 km along the X-direction (E–W), 15 km along the Y-direction (N–S) and 5 km along the vertical Z-direction, defining a volume of

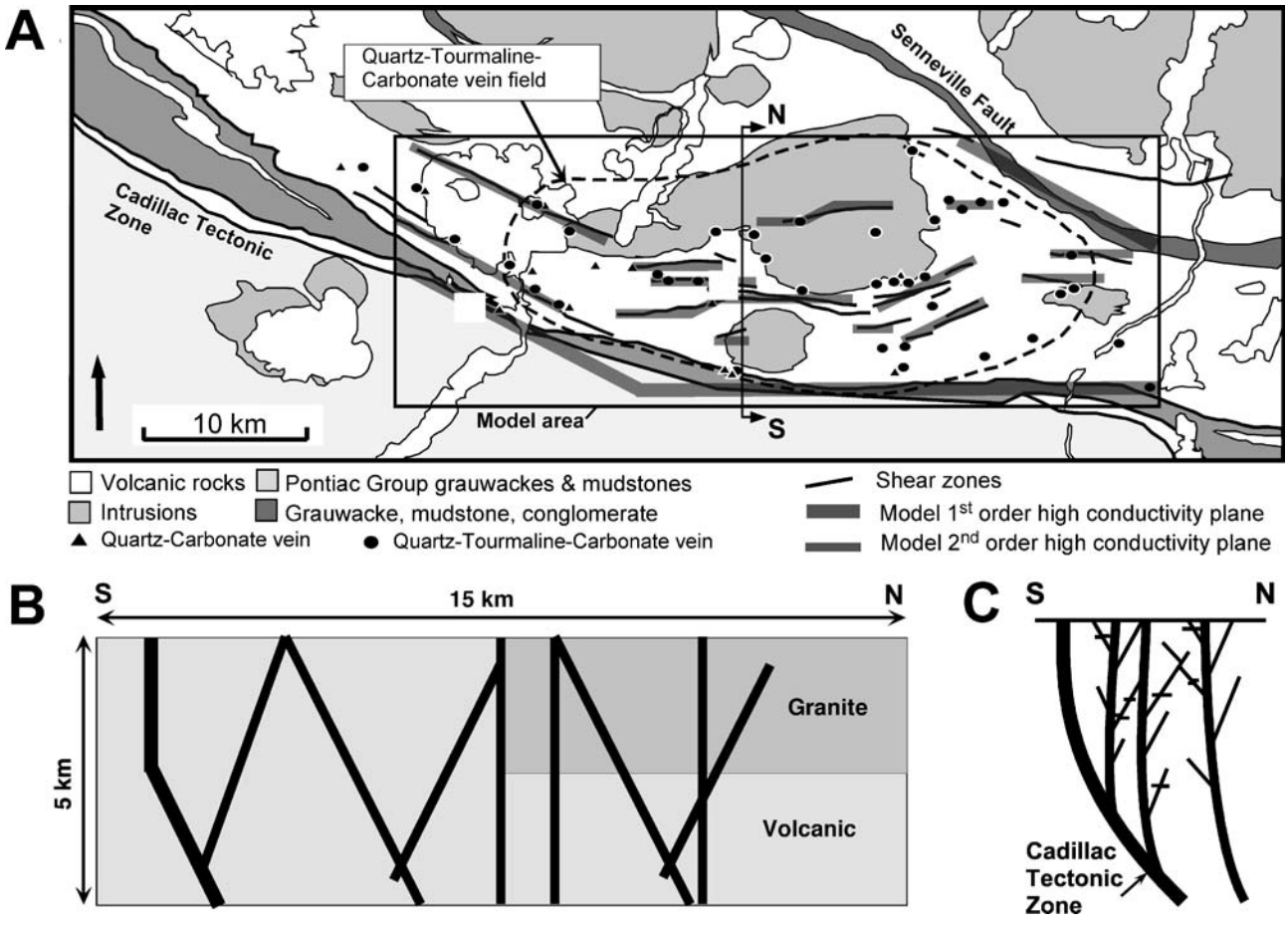

Fig. 5 **a** Simplified geology of the Val-d'Or area, with the outline of the quartz–tourmaline–carbonate vein field (modified from Robert 1994). The *rectangle* shows the surface area that is modelled in the study. In that modelled region, first-order (Cadillac tectonic zone and Senneville shear zone) and second-order shear zones are overlain by the trace of first- and second-order high-conductivity planes used in 3D modelling. The N–S cross-section is shown in **b**. **b** Cross-section (looking west) in the central part of the 3D model showing distribution of volcanic and granitic lithologies based on the Bourlamaque gravimetric signature (Jébrak et al. 1991). First- and second-order high-conductivity planes (same legend as in **a**) form a pattern of interconnected planes rooted or blind at the lower and upper boundaries of the 3D model. The pattern of high-conductivity planes is a schematic representation of the interpreted network of first- and second-order shear zones in the Val-d'Or vein field shown in **c**. **c** Interpreted pattern of interconnected shear zones in the Val-d'Or vein field (Robert et al. 1995)

3,375 km^3. A constraint in designing a 3D finite element grid onto which 2D fracture elements are superimposed is that the 3D and 2D elements must share common nodes. For the Val-d'Or area, the grid has to allow representation of the structural pattern interpreted for the vein field (Fig. 5c) and must be designed such that it can accommodate 2D elements representing E–W, N–S, 060° or 120° oriented fractures, having either a vertical or 60° dip to the north or the south. The model volume is therefore divided into 432,000 finite elements (180×120×20 elements along the *X*-, *Y*- and *Z*-directions, respectively) where each element is 250 m long by 125 m wide and by 250 m thick. The relative size of each element along the *X*-, *Y*- and *Z*-direction allows superimposing 2D elements representing fracture planes with the desired orientation.

All major shear zones in the Val-d'Or region have been simplified to 2D high-permeability plane segments that can be fitted onto the 3D grid (Fig. 5a). At depth, the extension of shear zones is interpreted from the strain fabric as well as from the interpreted interconnected pattern (Fig. 5b,c). The high-conductivity plane representing the Cadillac tectonic zone (Fig. 5b,c) has a 60° dip towards the north from Z=0 to Z=2,500 m and is vertical from Z=2,500 to Z=5,000 m, as indicated by seismic refraction for that major crustal shear zone (Green et al. 1990). High-conductivity planes are interconnected with other planes, and they can either reach the upper and/or lower boundaries of the model, or they can terminate within the model without reaching the upper or lower boundaries (Fig. 5b). For all simulations, the hydraulic properties of the high-conductivity planes are kept constant, with first-order high-conductivity planes (Fig. 5a,b) having a thickness ($2b$) of 100 m and a hydraulic conductivity (K) of 250 m year^{-1} and second-order high-conductivity planes (Fig. 5a,b) having a thickness ($2b$) of 30 m and a hydraulic conductivity (K) of 500 m year^{-1}.

These values are based on field characteristics of the shear zones and on typical hydrogeologic parameters, although there is no knowledge of the in situ hydraulic conductivity of shear zones at that mid-crustal depth.

Most rocks forming the Val-d'Or area are volcanic and show a small range of average $\delta^{18}O$ values (Beaudoin and Gagnon 2001) such that a uniform oxygen isotope composition ($\delta^{18}O$=6‰) is assumed for the matrix. The volcanic rocks have been assigned a hydraulic conductivity of 0.25 m year^{-1} (8×10^{-9} ms^{-1}), a value typical for kilometer-scale hydraulic conductivity in crustal rocks (Ingebritsen and Sanford 1998; Manning and Ingebritsen 1999). The Bourlamaque Batholith has likely physical properties that are different from the other rocks in the area. To study the effect of heterogeneities in the rock properties, several simulations were conducted where the Bourlamaque Batholith is represented as a volume of granitic rocks, with a $\delta^{18}O$=9‰ and a hydraulic conductivity of 0.025 m year^{-1} (8×10^{-10} ms^{-1}) to account for its massive structure (Fig. 5a,b), and with a thickness of a 2.5 km, from Z=2,500 to Z=5,000 m, as indicated by gravimetric studies (Jébrak et al. 1991). The very large contrast in hydraulic conductivity between the rock and the high-permeability planes (10^3 to 2×10^4) will lead to solute transport being dominated by advection in the planes and by diffusion in the rock matrix.

A constant oxygen isotope fractionation factor (α_k=1.004) is used based on hydrothermal fluid–rock experiments at 350°C (Cole et al. 1992). This isothermal hypothesis is supported by lack of a thermal gradient in the Val-d'Or vein field as described previously (Beaudoin and Pitre 2005). The reverse reaction rates (k_k) used in the simulation range from 10^{-5} to 10^{-6} year^{-1}, which is a range of values typical for water–rock exchange at 350°C (Cole et al. 1992; Criss et al. 1987; Cole and Chakraborty 2001).

The regional oxygen isotope study of the Val-d'Or vein field (Beaudoin and Pitre 2005) identified two mixing end-member fluids: (1) a supracrustal fluid with a long history of water–rock oxygen isotope exchange within the volcanic rock pile and with a maximum $\delta^{18}O$ value of 3.9‰ and (2) a deep-seated, metamorphic fluid with a minimum $\delta^{18}O$ value of 8.5‰. Beaudoin and Pitre (2005) suggested that this supracrustal fluid was trapped in the volcanic pile pores and fractures. Based on these data, we assigned a $\delta^{18}O$ value of 4‰ for the interstitial fluid filling porosity in the matrix and a value of 9‰ for the infiltrating fluid in all simulations.

The choice of boundary conditions for fluid flow greatly influences the simulated oxygen isotope isopleths (Badertscher et al. 2002; Beaudoin and Therrien 1999). Four different combinations of top and bottom boundary conditions for fluid flow have been investigated (Fig. 6) that represent geologically meaningful settings. For all cases, lateral boundaries of the simulation domain are assumed impermeable. For Scenario 1, the entire top and bottom boundaries are permeable and are assigned prescribed hydraulic heads that cause fluid inflow at the bottom of the domain and outflow at the top (Fig. 6a). For Scenario 2, the top of the domain is a permeable outflow boundary (Fig. 6b), while the bottom is assumed impermeable except along the trace of the Cadillac tectonic zone, where a prescribed hydraulic head is assigned to allow fluid inflow at that location. For Scenario 3, the entire top and bottom boundaries of the model are impermeable except along the trace of the Cadillac tectonic zone where inflow and outflow are forced by imposing hydraulic heads (Fig. 6c). Scenario 4 corresponds to a permeable inflow boundary at the bottom, with outflow at the top restricted to the trace of the Cadillac tectonic zone, the rest of the surface being considered impermeable (Fig. 6d). Several simulations have been conducted for each scenario, and representative results are presented below.

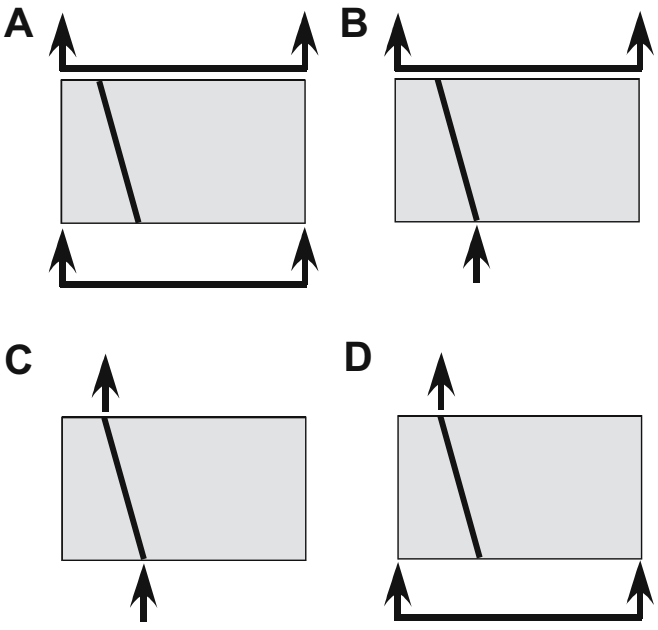

Fig. 6 Schematic boundary condition scenarios at the *bottom* and *top* of the 3D model viewed in cross-section looking west, with the trace of the Cadillac tectonic zone. In all cases, the side boundaries of the model are considered impermeable. **a** The lower and upper boundaries are permeable, and fluid inflow is across the bottom of the model whereas outflow is at the top as shown by the bar with arrows. **b** The lower boundary is impermeable but along the trace of the Cadillac tectonic zone where the lower boundary is permeable and allows fluid inflow (*arrow*). The upper boundary is permeable and allows fluid outflow across the model surface (*bar with arrows*). **c** The lower and upper boundaries are impermeable but along the trace of the Cadillac tectonic zone where inflow and ouflow is allowed (*arrow*). **d** The lower boundary is permeable allowing fluid inflow across the base of the model (*bar with arrows*). The upper boundary is impermeable but along the trace of the Cadillac tectonic zone where outflow of fluids is shown by the *arrow*

Scenario 1

The boundary conditions for Scenario 1 correspond to a block of crustal rocks infiltrated by hydrothermal fluids from below. The simulations show narrow, highly focused, oxygen isotope reaction zones near the high-permeability planes that reach the upper surface of the model (Fig. 7). Comparing Fig. 7b and c, the system appears to have reached steady-state between 50 and 100 ka, a time-scale

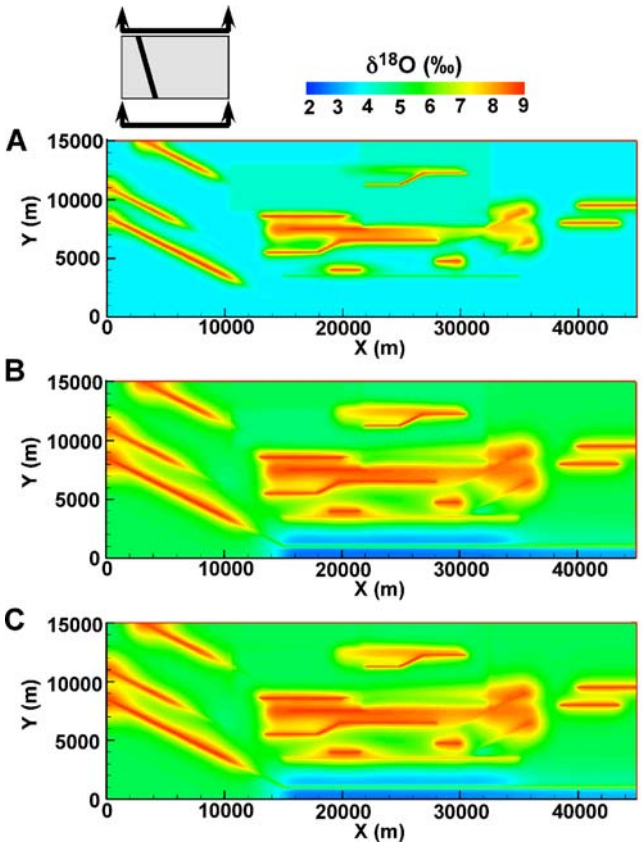

Fig. 7 Simulated $\delta^{18}O_{fluid}$ values for boundary conditions of Scenario 1 (Fig. 6a), for a hydraulic head of 200 m, n=0.05, k_k=10^{-6} year^{-1} (simulation #v2ig), and after 5 ka (**a**), 50 ka (**b**) and 100 ka (**c**)

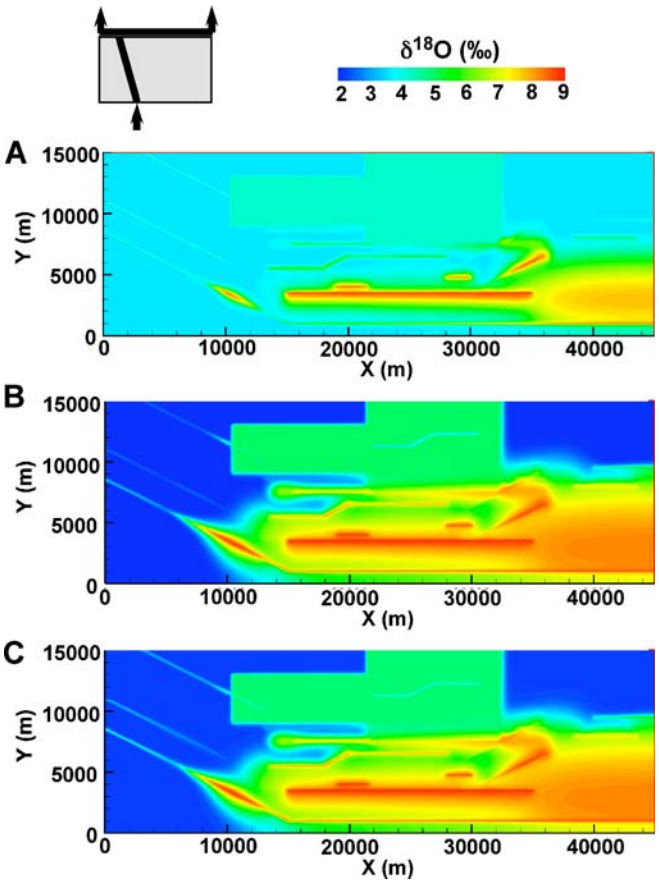

Fig. 8 Simulated $\delta^{18}O_{fluid}$ values for boundary conditions of Scenario 2 (Fig. 6b), for a hydraulic head of 5,000 m, n=0.05, k_k=10^{-6} year^{-1} (simulation #v4igp), and after 5 ka (**a**), 50 ka (**b**) and 100 ka (**c**)

mostly determined by the value of the reverse rate of reaction (k_k=10^{-6} year^{-1}) at which time oxygen isotope equilibrium is reached between the matrix and the interstitial fluid. The boundary conditions of Scenario 1 (Fig. 7) fail to produce the oxygen isopleth pattern determined from the Val-d'Or vein field (Fig. 2). The highly focused flow and reaction, however, clearly show the location of the high-permeability planes reproducing shear zones mapped in the field (Fig. 5a).

Scenario 2

Scenario 2 attempts to reproduce the oxygen isotope composition of fluids that are channelled into the vein field from below only along the trace of the Cadillac tectonic zone (Fig. 8). The upper boundary of the model is permeable and allows outflow, representing a crustal segment infiltrated along the linear trace of the Cadillac tectonic zone at the otherwise impermeable lower boundary of the model, as well as fluid flux across the rock matrix towards the upper permeable boundary. Simulation results for three different times, 5, 50 and 100 ka (Fig. 8a–c), show the effect of variable lithologies on water–rock exchange, with the boundary conditions allowing little fluid flow in the northern part of the vein field (upper part of each panel). At 100 ka, the fluid has reached equilibrium with volcanic rocks ($\delta^{18}O$=6‰) at a value of 2‰, whereas fluid reacting with rocks representing the Bourlamaque batholith ($\delta^{18}O$=9‰) reaches 5‰ as a consequence of the oxygen isotope fractionation of 1.004 (Fig. 8c). The pattern of oxygen isopleths is controlled by the high-permeability planes connected with the plane representing the Cadillac tectonic zone (Fig. 8). The boundary conditions of Scenarios 1 and 2 fail to produce oxygen isotope isopleths at high angle to the major crustal shear zones.

Scenario 3

The third scenario involves fluid channelling along the trace of major shear zones, the Cadillac tectonic zone and the Senneville shear zone, that extend vertically across the whole domain (Fig. 6c). This scenario implies that the lower and upper boundary conditions are impermeable to flow except where a fluid source (bottom) or a fluid drain (top) has been added along the trace of the two major crustal shear zones. All other high-permeability planes in the model participate to fluid flow but they are not in direct connection with neither the fluid source nor the fluid drain. In Fig. 9, we present modelling results where the Cadillac tectonic zone (Fig. 5) cuts E–W across the model in the

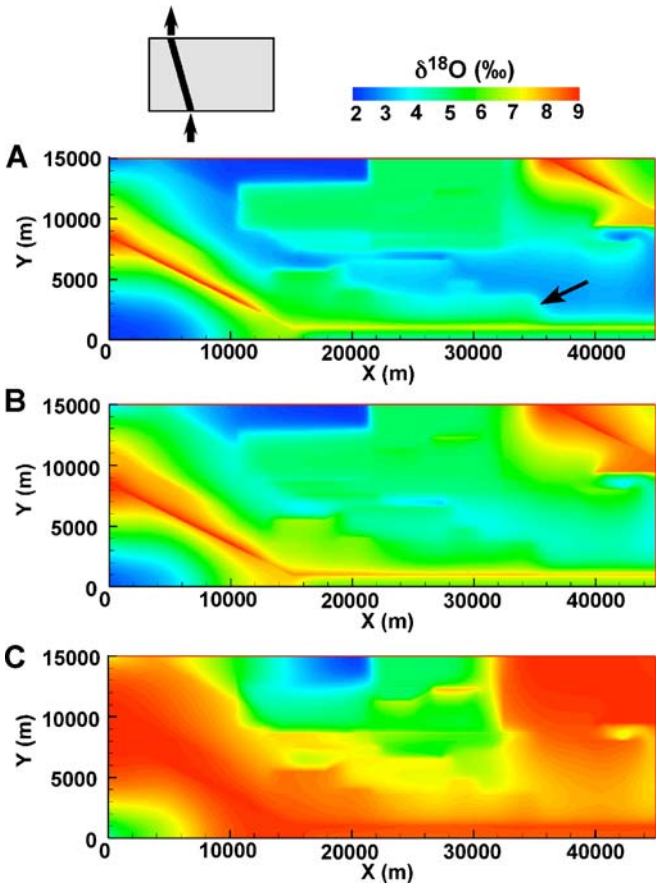

Fig. 9 Simulated $\delta^{18}O_{fluid}$ values for boundary conditions of Scenario 3 (Fig. 6c), for a hydraulic head of 1,000 m, n=0.05, k_k=10^{-6} year^{-1} (simulation #v1i2g), and after 0.1 Ma (**a**) where the *arrow* points to an isopleth at high angle to the hydraulic drain along the trace of the Cadillac tectonic zone, 1 Ma (**b**) and 5 Ma (**c**)

southern part of each panel, as in Scenarios 1 and 2, and where the Senneville shear zone (Fig. 5) is represented by a NE–SW zone of high permeability in the NE corner of the model. These boundary conditions have profound effects on the fluid flow and oxygen isotope exchange patterns because the fluids infiltrating the model can only be drained along the trace of the major shear zones cutting across the impermeable upper boundary. As a result, broad zones of oxygen isotope exchange develop on both sides of the trace of the major crustal shear zones (Fig. 9c).

The detailed shape of the oxygen isotope isopleths depends on the position and interconnection of the high-permeability planes and also on matrix permeability contrasts represented in the model (Fig. 5b). In particular, at 5 Ma (Fig. 9c), the NE corner of the model develops a rectangular pattern of oxygen isopleths as a result of the permeability contrast (10×) imposed along the N–S boundary of model elements representing the Bourlamaque batholith and because of a nearby E–W second-order high-conductivity plane (Fig. 5b). There are similarities in the oxygen isopleth pattern from the field (Fig. 2) and from model results of Scenario 3. Because fluids are drawn towards the hydraulic drain along the trace of the Cadillac tectonic zone, oxygen isopleths develop a pattern at high angle to the drain (Fig. 9a). In addition, draining along the trace of the Cadillac tectonic zone and the Senneville shear zone creates a valley of lower $\delta^{18}O$ values in the southeast corner of the modelled area (Fig. 9c), similar to the pattern mapped from the field (Fig. 2). There are, however, important differences between modelling results using Scenario 3 boundary conditions and the oxygen isopleth map shown in Fig. 2. Scenario 3 boundary conditions (Fig. 9) fail to reproduce the zone of high $\delta^{18}O$ values in the south-central part of the vein filed, north of the Cadillac tectonic zone (Fig. 2). In addition, the trace of the Cadillac tectonic zone in the western part of the vein field is characterized by a broad zone of $\delta^{18}O$ values (Fig. 9c) unlike the pattern shown in Fig. 2 that is characterized by a tongue of low $\delta^{18}O$ values towards the southwest.

Scenario 4

The influence of several model parameters is shown in Fig. 10 for Scenario 4. The three simulation results of Fig. 10 are shown at the same time step (100 ka), using the same porosity (0.05) and hydraulic head (200 m) imposed across the permeable base of the model. Figure 10a shows the fluid oxygen isotope isopleths when the model is infiltrated at the base from a permeable boundary but where fluids are allowed to drain out only across the trace of the Cadillac tectonic zone. As shown in Fig. 10a, a broad zone of higher $\delta^{18}O$ values has developed in the south-central part of the model to the north of the fluid drain. Adding a hydrogeological unit corresponding to the Bourlamaque Batholith with a higher $\delta^{18}O$ value (9‰) and a hydraulic conductivity (0.025 m year^{-1}) ten times lower than that of the surrounding volcanic rocks causes water in that region to reach isotope equilibrium with the rocks because of the low rate of transport away from the hydraulic drain in the south (Fig. 10b). If the impermeable upper boundary is pierced by an additional linear permeable drain, along the trace of the Senneville shear zone in the NE corner, fluids are drawn into that drain forming a new zone of oxygen isotope exchange (Fig. 10c). The configuration of the hydraulic drains therefore has major influence of the fluid flow paths and reaction. This is clearly shown by comparing with results from Scenario 1 (Fig. 7c) and Scenario 2 (Fig. 8c).

Figure 11 shows the results of the numerical simulation that most closely reproduce the oxygen isotope isopleths measured in the Val-d'Or vein field (Fig. 2). To simulate an oxygen isopleth pattern most resembling that measured in the field, the boundary conditions of Scenario 4 (Fig. 6d) are imposed with fluid drains across the impermeable top boundary of the model along the trace of the E–W Cadillac tectonic zone in the south and along that of the Senneville shear zone in the northeast corner of the modelled area. The pattern of oxygen isopleths obtained after 5 Ma (Fig. 11d) comprises a zone of high $\delta^{18}O$ values in the south-central

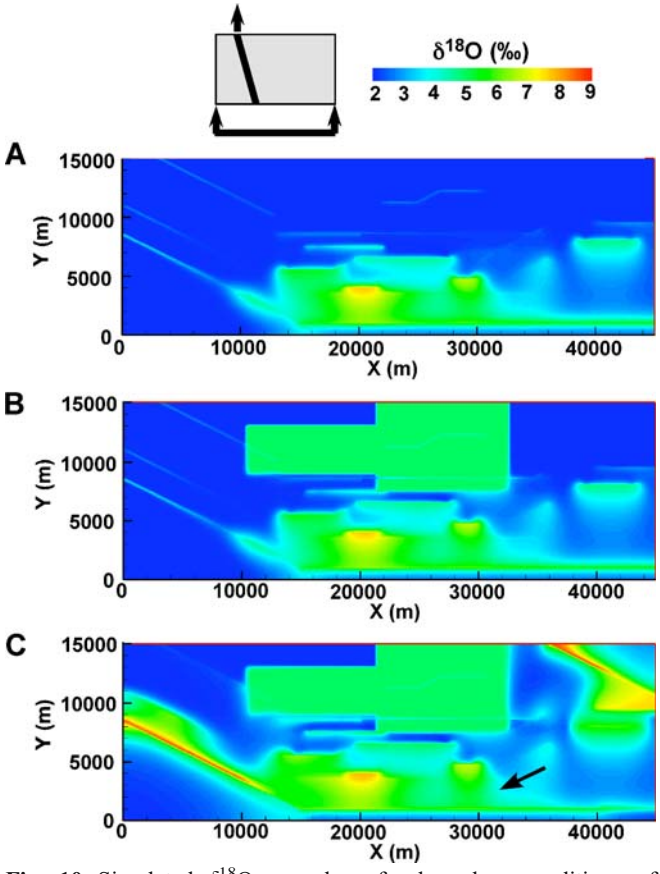

Fig. 10 Simulated $\delta^{18}O_{fluid}$ values for boundary conditions of Scenario 4 (Fig. 6d), for a hydraulic head of 200 m, n=0.05, k_k=10^{-6} year^{-1}, and after 100 ka. Simulations are for the following: **a** One hydrostratigraphic unit representing volcanic rocks (simulation #v3i). **b** Same as **a** but with the addition of a second hydrostratigraphic unit representing the Bourlamaque batholith in the north (simulation #v3ig). **c** Same as **b** but with the addition of a second hydraulic drain in the NE corner along the trace of the Senneville shear zone (simulation #v3i2g). The *arrow* points to an isopleth at high angle to the hydraulic drain along the trace of the Cadillac tectonic zone

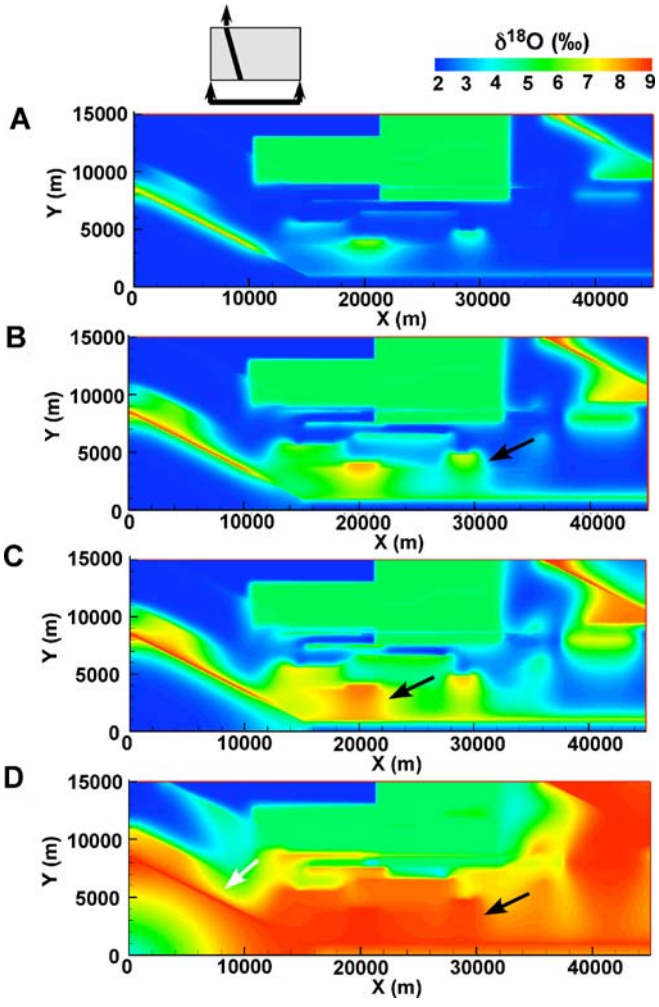

Fig. 11 Simulated $\delta^{18}O_{fluid}$ values for boundary conditions of Scenario 4 (Fig. 6d), for a hydraulic head of 200 m, n=0.01, k_k=10^{-5} year^{-1} (simulation #k2r5h2), and after 0.1 Ma (**a**), 0.5 Ma (**b**), 1 Ma (**c**) and 5 Ma (**d**). *Black arrows* point to isopleths at high angle to the hydraulic drain along the trace of the Cadillac tectonic zone, whereas the *white arrow* highlights a tongue of low $\delta^{18}O_{fluid}$ values at high angle to the trace of the Cadillac tectonic zone

part of the vein field with oxygen isopleths at high angle to the trace of the Cadillac tectonic zone (Fig. 11, black arrows), a valley of lower $\delta^{18}O$ values towards the southeast of the vein field, a ridge of high $\delta^{18}O$ values in the northeast corner of the vein field and a zone of high $\delta^{18}O$ values along the northwestern trace of the Cadillac tectonic zone that is cut by a tongue of low $\delta^{18}O$ values towards the southwest (Fig. 11, white arrow), as shown for field data in Fig. 2. Modelling results using Scenario 4 boundary conditions (Fig. 11), however, fail to replicate the broad zone of high $\delta^{18}O$ values in the western part of the vein field (Fig. 2).

Importance of fluid drains

A feature of oxygen isopleths for hydrothermal fluids shown in Fig. 2 is that some isopleths are at high angle to the major crustal shear zones. This feature could be a consequence of isopleths either being cut by displacement along the major crustal shear zones after cessation of gold mineralization or a consequence of fluid flow and isotope exchange being controlled by the major shear zones. Although it cannot be rejected, the hypothesis of isopleths being cut by the shear zones is considered unlikely because small gold-bearing veins are found occasionally in the Pontiac sub-province metasedimentary rocks south of the Cadillac tectonic zone. Our modelling results, however, show that fluids drawn towards a hydraulic drain such as in Scenarios 3 (Fig. 9a) and 4 (Figs. 10c and 11b–d) will form zones of higher $\delta^{18}O$ values by reaction and transport that are characterized by isopleths at high angle to the fluid drain. Isopleths at high angle to a major crustal shear zones were also mapped in the Kokanee Ag–Pb–Zn vein field (Beaudoin et al. 1992b) and were reproduced by 3D fluid reaction and transport numerical modelling (Beaudoin and Therrien 1999). Isopleths at high angle to crustal shear zones therefore most likely indicate fluid reaction and

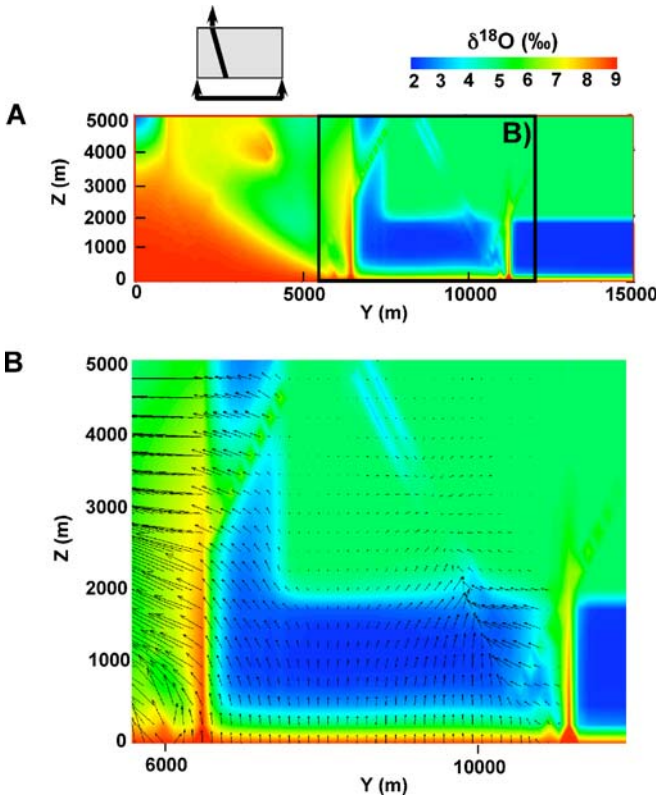

Fig. 12 **a** Fluid $\delta^{18}O$ values for a S (Y=0 m)–N (Y=15,000 m) cross-section at X=22,500 m, for Scenario 4 (simulation #k2r5h2) at 1 Ma (Fig. 11c). *Black rectangle* outlines the area shown in **b**. **b** Part of **a** where fluid $\delta^{18}O$ values are overlain by vectors whose length is proportional to fluid velocity (*black arrows*)

transport controlled by a hydraulic drain located along the trace of the shear zone. Isopleths at high angle to the major crustal shear zones arise from advection-dominated flow and reaction in first- and second-order shear zones. Fluid in the shear zones is dominated by the composition of the infiltrated fluid higher up in the vein field. Where the shear zones are not connected to a hydraulic drain, fluids advect at low velocity through the porous matrix therefore allowing reaction along the flow path between the shear zone and the hydraulic drain (Fig. 12a).

Modelling results highlight the importance of not only deciphering the source of fluids and their solutes, the common practice applied by most researchers, but also determining the fluid outflow regions because these hydraulic drains have a determinant control on transport and reaction between the host rocks and the hydrothermal fluids. A consequence of having a linear drain within an impermeable upper boundary, as in Scenarios 3 and 4, is that fluids within the vein field have to flow towards the lower hydraulic head area. Figure 12a is a S–N cross-section at 1 Ma in the middle of Fig. 11c that shows the increased transport and reaction near the hydraulic drain in the south (Cadillac tectonic zone) that is caused lateral flow towards the hydraulic drain (Fig. 12b). Fluids in the northern part of the model (Y=15,000 m) have lower velocities because they must advect through a low-permeability matrix towards the low hydraulic head region (Fig. 12b). In that example, there is no effect from the hydraulic drain along the trace of the Senneville shear zone that reaches the northern boundary of the model about 10 km east of Fig. 12a cross-section. For these high-permeability planes far from the hydraulic drain, such at Y=11,500 m and Z=0 m, fluid oxygen isotope composition is dominated by that of the infiltrating fluid at the base. Fluid oxygen isotope composition reaches isotope equilibrium with the rock matrix surrounding the plane toward the top of the model because low-velocity fluid advection in the surrounding porous rock matrix, as shown by velocity values too small to display in Fig. 12b, which leads to a system dominated by reaction and diffusion.

The control of low hydraulic head fluid drains on fluid transport probably explains the abundance of orogenic gold deposits to the south and east of the Bourlamaque batolith (Fig. 2) not only because of lithological contrast but also because of the position of the linear low hydraulic head controlling fluid flow. As a consequence, it is predicted that other significant gold deposits should exist in the northeast area of the Val-d'Or vein field, such as the Beaufor Mine which contains more than 30 t Au in past-production and reserves, making it the second largest gold deposit in the Val-d'Or vein field after the Sigma Mine (about 300 t Au).

Discussion

Implications for NW–SE shear zones in the Abitibi sub-province

Modelling results suggest a significant control of fluid flow by the Senneville shear zone, a NW–SE, south-verging, steeply dipping major shear zone (Daigneault 1996). The Senneville shear zone contains strike-slip lineations related to dextral shearing near the Bourlamaque batholith, and down-dip lineation to the east where its strike curves to an E–W orientation (Daigneault 1996). In the Abitibi sub-province, the down-dip lineation in E–W shear zones is associated to N–S shortening, and this shortening event is commonly overprinted by dextral shearing that is most intense in NW–SE shear zones (Desrochers and Hubert 1996; Daigneault et al. 2002; Robert 1989; Hubert et al. 1984). Orogenic gold is associated with the earlier N–S shortening along E–W structures, although several NW–SE shear zones also contain gold deposits, such as the Cameron tectonic zone which is 150 km north of Val-d'Or (Roy et al. 1997). In the Cameron tectonic zone, several gold deposits are in E–W segments characterized by down-dip lineation overprinted by intense strike-slip deformation in NW–SE segments (Roy et al. 1997). These E–W segments within NW–SE shear zones could have been E–W shear zones dismembered or reoriented during later dextral NW–SE strike-slip shearing (Roy et al. 1997). This interpretation is supported by our simulations that indicate that the NW–SE Senneville shear zone most likely drained hydrothermal fluids

during formation of the Val-d'Or vein field under N–S compressive stress. These lines of evidence suggest that some of the NW–SE shear zones were active during the orogenic gold hydrothermal systems and represent an exploration target in the Abitibi sub-province that has been less explored than the better known E–W shear zones.

Estimate of fluid flux

The volume of fluid containing 1 ppb Au in solution, at 350°C and 0.17 GPa with a density of 0.827 t m^{-3} (http://webbook.nist.gov/chemistry/fluid/), required to precipitate the 0.9 kt Au of the Val-d'Or vein field is 1,088 km^3 which is about 1/3 of the volume of rocks hosting the veins. This volume is comparable to the volume of fluids (~6,000 km^3) estimated to have flowed through the major crustal shear zones in the Abitibi (Kerrich et al. 1987). That volume of fluid is a minimum because the amount of gold taken into account is the mineral resource that does not include lower grade or smaller gold deposits, as well as deposits that have yet to be discovered. The total amount of gold deposited in the Val-d'Or vein field is unknown, but it is instructive to compare the gold resource (0.9 kt Au) to the amount of gold that would be contained in the 3,375 km^3 of rocks of the model with a grade of 1 ppb, that is 9.1 kt Au or ten times more than the gold resource.

Under the conditions of the simulation shown in Fig. 11, 0.0122 km^3 $year^{-1}$ of fluid flowed across the lower and upper boundaries of the model, such that gold in the Val-d'Or vein field could have been deposited in about 89.2 ka. This value for the duration of the Val-d'Or is similar to the 10^4- to 10^5-year time-scale estimated from tourmaline abundance and boron solubility for the Sigma deposit (Garofalo 2000). If fluids were formed by greenschist–amphibolite prograde metamorphism in a region with an area of 1,000 km^2, then a rock column 6.7 km thick yielding 5 wt.% H_2O is required to generate the 1,088 km^3 of hydrothermal auriferous fluid with 1 ppb Au. Using a prograde burial rate for a convergent orogen of 0.07 m $year^{-1}$ (Perchuk et al. 1999), it would take about 95 ka to cross a devolatilization isograd. Coupled thermal–mechanical models using average convergence rates (0.01 m $year^{-1}$) indicate that a 6.7-km-thick rock column will cross the 550°C isotherm in about 3.4 Ma (Jamieson et al. 1998). Under the model conditions shown in Fig. 11, the Val-d'Or vein field fluid oxygen isopleths are reproduced after 1–5 Ma (Fig. 11c,d). The calculated duration of the hydrothermal system from different methods is within one order of magnitude such that this duration is likely a good approximation. The calculations indicate that a pulse of hydrothermal fluids forming major orogenic gold vein fields most likely will form under special conditions, perhaps involving rapid convergence and burial. This would cause an intense pulse of metamorphic fluid from dewatering of the underlying rock column. This very short time-span for fluid generation and flux is comparable to the time frame for the formation of the Juneau gold belt (Alaska) in about 3.7 Ma (Goldfarb et al. 1991; Miller et al. 1994).

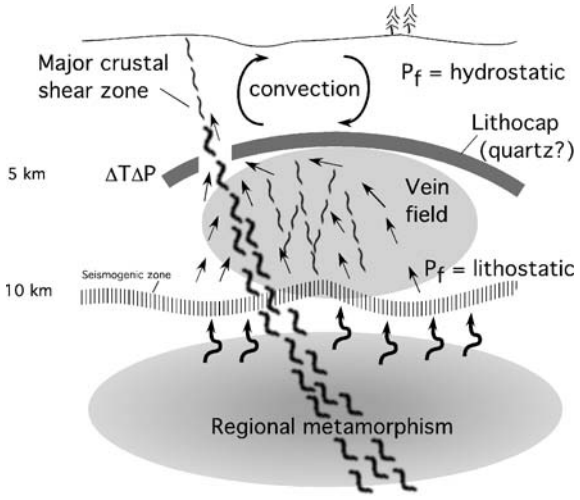

Fig. 13 Conceptual model showing fluids formed during prograde regional metamorphism that infiltrate across a broad zone at the base of the vein field. Lithostatic fluid pressure builds up because fluid flow is impeded by a low-permeability lithocap that separates the overpressured domain from the hydrostatic fluid pressure regime above. The major crustal shear zone breaches the low-permeability barrier intermittently, allowing fluids that precipitated dissolved gold to escape the vein field, allowing new gold-bearing fluids to enter the vein field. The shear zone breach in the low-permeability barrier creates a low hydraulic head that controls the schematic fluid flow paths (*arrows*) in the vein field

What is the role of major crustal shear zones?

Our numerical modelling results in the Val-d'Or orogenic gold vein field and a previous study of the Kokanee Ag–Pb–Zn vein field (Beaudoin and Therrien 1999) indicate that fluid flow in vein fields under sub- to supra-lithostatic fluid pressure is controlled by similar boundary conditions irrespective of the compressive or extensional tectonic setting. These boundary conditions thus represent major controls on fluid flow and water–rock exchange and provide challenging interpretations of the permeability parameters in a transition zone at the edge of the fossilized vein fields. The lower boundary condition represents a permeable crustal domain pervasively infiltrated from below by rising metamorphic fluids (Fig. 13). During intense tectonic events, pulses of metamorphic fluids are likely produced at depth by prograde dehydration mineral reactions within a broad zone of 1,000s km^2 that generate transient increases in porosity that are likely to enhance hydraulic conductivity and to allow fluid migration (Tenthorey and Cox 2003) that might propagate upward as fluid pressure waves (Connolly 1997). This is likely to result in short-lived pulses of metamorphic fluid that is consistent with the short duration for the hydrothermal

system estimated from our fluid flow results (10^5 years), tourmaline abundance and boron solubility at the Sigma deposit (10^4–10^5 years; Garofalo 2000) and dating in the twit Juneau gold belt, Alaska (Goldfarb et al. 1991; Miller et al. 1994).

The upper impermeable boundary separates the deep-seated fluid regime, under sub- to supra-lithostatic fluid pressure, from the surficial fluid regime under hydrostatic pressure (Sibson and Scott 1998; Zoback and Townend 2001; Cox 2005). This impermeable boundary is critical to impede upward fluid flow, build fluid pressure underneath (Cox et al. 2001), induce hydraulic fracturing and favour fluid–rock exchange (Fig. 13). Such impermeable layers have been shown to control fluid flow in magmatic–epithermal systems, ancient volcanogenic massive sulphide deposits and to seal hydrothermal fluid reservoirs of active submarine hot springs (Galley 1993). The upper boundary can be an impermeable lithological unit or a layer where mineral precipitation seals permeability. The depth and thickness of this impermeable layer depend on the tectonic and fluid regimes (Sibson and Scott 1998). Mineral precipitation is likely to be dominated by the solubility of quartz, which increases with temperature and pressure. The transition zone between the surficial hydrostatic pressure regime and the underlying lithostatic pressure regime will be a region where a steep pressure gradient exists (Sibson and Scott 1998), forcing quartz precipitation because of the lower solubility of quartz at lower pressure. The upper impermeable transition zone fluid pressure gradient also coincides with a steep temperature gradient because the surficial hydrostatic fluid regime will have a lower temperature than the deep-seated fluids migrating upward along a temperature path. This temperature gradient will also cause precipitation of quartz, or other minerals with a prograde temperature solubility, to cement the impermeable layer.

The crustal-scale faults are permeable regions that cut the overlying low-permeability pressure regime transition zone (Fig. 13). Episodic seismic deformation along these faults creates porosity and temporarily increases permeability across the cemented impermeable transition zone. This causes a region of lower hydraulic head at the top of the region under sub- to supra-lithostatic fluid pressure that drain fluids out of the vein field. Our model complements Cox et al.'s (2001) interpretation that rising fluids were ponded beneath a low-permeability domain but without an outflow component for the system. Cox (2005), however, considers that rupturing the low-permeability seal will lead to the most intense episodes of flow. We propose therefore that crustal-scale faults drain hydrothermal fluids out of vein fields, and the geometry of that hydraulic drain controls the shape of the oxygen isotope isopleths from hydrothermal fluids. High fluid/rock ratios are required to accumulate gold into veins, such that fluids must flow out of the vein field, along hydraulic drains. It is suggested that hydrothermal fluids deposited gold in fractures prior to escaping the vein field, therefore explaining the paradox of a strong spatial association between orogenic gold deposits and the crustal shear zones, the similar fluid properties (Neumayr et al. 2000; Neumayr and Hagemann 2002), and yet the small number and size of deposits hosted in these major shear zones. In active seismic regions, earthquakes are commonly accompanied by changes in the hydrogeologic regime, testifying to the release of large volumes of water into the segment of the crust under hydrostatic fluid regime (Irwin and Barnes 1980; Muir-Wood 1994).

Our modelling results in the Val-d'Or orogenic gold and Kokanee Ag–Pb–Zn (Beaudoin and Therrien 1999) vein fields offer a new interpretation of the role of major crustal shear zones during formation of the precious and base metal deposits. Both vein fields are interpreted to have formed by overpressured fluids, albeit in contrasted tectonic regimes. The Kokanee vein field formed during crustal extension (Beaudoin et al. 1992a,b; Carr et al. 1987), and the Val-d'Or vein field and other orogenic gold districts formed in compressive or transpressive tectonic regimes (Groves et al. 1998; Goldfarb et al. 2001; Robert and Brown 1986). The Kokanee Ag–Pb–Zn vein field formed under suprahydrostatic to near-lithostatic fluid pressure in an extensional tectonic regime (Beaudoin et al. 1992b), whereas the Val-d'Or vein field formed under lithostatic to supralithostaic fluid pressure in a compressional tectonic regime (Robert et al. 1995). The vein fields are interpreted to have formed towards the base of the seismogenic crust near major crustal faults (Boullier and Robert 1992; Beaudoin et al. 1992b; Groves et al. 1998; Sibson et al. 1988). In both stress systems, high fluid pressure can develop below a low-permeability transition zone that separates the hydrostatic fluid pressure regime from the underlying suprahydrostatic to lithostatic fluid regime in extensional tectonic setting or the lithostatic to supralithostatic fluid regime in compressional environments (Sibson and Scott 1998). Comparing these two contrasted geodynamic environments should therefore provide insights into fluid flow in overpressured vein fields independent of tectonic setting.

It is significant that the Kokanee and Val-d'Or vein fields formed under conditions of sub-lithostatic to supra-lithostatic fluid pressure. It is thus concluded that in vein fields formed under high fluid pressure irrespective of the tectonic settings, the role of the major shear zones spatially associated with mineralization is to drain hydrothermal fluids across the impermeable barrier required for the high fluid pressure regime. This conclusion is consistent with the spatial association of the veins with major crustal shears that have been infiltrated by the same hydrothermal fluids (Neumayr et al. 2000; Neumayr and Hagemann 2002) that formed mineralization near the shear zones. The paradox of this close spatial association with shear zones but lacking significant metal accumulation is interpreted to indicate that the fluids had precipitated a major part of the metals in solution in other veins on their way towards the hydraulic drain provided by the crustal shear zone.

Conclusions

Fossil fluid flow patterns can be mapped at the scale of a vein field using oxygen isotopes. 3D numerical modelling

of oxygen isotope transport and reaction shows that to reproduce the fluid flow patterns mapped in vein fields at high fluid pressure, it is necessary to impose a permeable lower boundary to the model which is infiltrated by fluids from below. This lower permeable boundary allows infiltration of short-lived pulses of metamorphic hydrothermal fluids carrying metals in solution. Fluids infiltrating from below are drawn into zones of dilation where metals are deposited in an interconnected network of subsidiary shears. The other critical condition is an impermeable upper boundary that is made permeable along linear hydraulic drains that represent the major crustal shear zones. The upper impermeable barrier arrests fluid flow and separates the high fluid pressure regime below from the hydrostatic fluid regime above. The high, local fluid–rock ratios require that fluids flow out of the vein field through the evolving and interconnected network of shear zones and by advection through the rock matrix. Episodic movements along the crustal shear zone create breaches in the impermeable barrier that allow fluid flow out of the vein field.

It is thus concluded that the major crustal faults so conspicuous in vein fields under sub- to supra-lithostatic fluid regimes, irrespective of compressive or extensional tectonic setting, play the role of a hydraulic drain across an upper impermeable barrier. They are not the sole channel controlling migration of hydrothermal fluids from their source to the site of economic mineral deposits as had been intuitively thought. Recognizing the role of major crustal faults as drains of hydrothermal fluids, instead of a source, should have major implications in the exploration for the mineral deposits associated spatially to the major crustal shear zones. Recognition of low-permeability barriers, perhaps as cemented cap rocks, near the crustal shear zones could indicate buried mineral resources in a vein field beneath.

Acknowledgements This research has been supported by a research grant from the Fonds québécois de la recherche sur la nature et les technologies to the research team MEDEF and by Natural Sciences and Engineering Research Council of Canada Discovery grants to GB and RT. Their long-term support is gratefully acknowledged. Detailed and constructive reviews by S.F. Cox, R.J. Goldfarb and R. Weinberg helped improve significantly this paper.

References

Badertscher NP, Beaudoin G, Therrien R, Burkhard M (2002) Glarus overthrust: a major pathway for the escape of fluids out of the Alpine orogen. Geology 30:875–878

Beaudoin G, Therrien R (1999) Sources and drains: major controls of hydrothermal fluid flow in the Kokanee Range, British Columbia, Canada. Geology 27:883–886

Beaudoin G, Gagnon Y (2001) Oxygen isotope cross-section of the synvolcanic VMS hydrothermal system of the Val-d'Or camp. In: GAC-MAC annual meeting, program with abstract, p 9

Beaudoin G, Pitre D (2005) Stable isotope geochemistry of the Archean Val-d'Or (Canada) orogenic gold vein field. Miner Depos 40:59–75

Beaudoin G, Roddick JC, Sangster DF (1992a) Eocene age for Ag–Pb–Zn–Au vein and replacement deposits of the Kokanee range, Southeastern British Columbia. Can J Earth Sci 29:3–14

Beaudoin G, Taylor BE, Sangster DF (1992b) Silver–lead–zinc veins and crustal hydrology during Eocene extension, southeastern British Columbia, Canada. Geochim Cosmochim Acta 56:3513–3529

Boullier A-M, Robert F (1992) Paleoseismic events recorded in Archaean gold–quartz vein networks, Val d'Or, Abitibi, Quebec, Canada. J Struct Geol 14:161–179

Bowman JR, Willett SD, Cook SJ (1994) Oxygen isotopic transport and exchange during fluid flow: one-dimensional models and applications. Am J Sci 294:1–55

Carr SD, Parrish RR, Brown RL (1987) Eocene structural development of the Valhalla Complex, southeastern British Columbia. Tectonics 6:175–196

Cole DR, Chakraborty S (2001) Rates and mechanisms of isotopic exchange. In: Valley JW, Cole DR (eds) Stable isotope geochemistry. The Mineralogical Society of America, Washington, pp 83–224

Cole DR, Ohmoto H, Jacobs GK (1992) Isotopic exchange in mineral–fluid systems: III. Rates and mechanisms of oxygen isotope exchange in the system granite–H_2O±NaCl±KCl at hydrothermal conditions. Geochim Cosmochim Acta 56:445–466

Connolly JAD (1997) Devolatilization-generated fluid pressure and deformation-propagated fluid flow during prograde regional metamorphism. J Geophys Res 102:18149–18173

Couture J-F, Pilote P, Machado N, Desrochers J-P (1994) Timing of gold mineralization in the Val-d'Or district, southern Abitibi Belt: evidence for two distinct mineralizing events. Econ Geol 89:1542–1551

Cox SF (2005) Coupling between deformation, fluid pressures, and fluid flow in ore-producing hydrothermal systems at depth in the crust. In: Hedenquist JW, Thompson JFH, Goldfarb RJ, Richards JP (eds) One hundredth anniversary volume. Society of Economic Geologists, Littleton, CO, pp 39–75

Cox SF, Ruming K (2004) The St Ives mesothermal gold system, Western Australia—a case of golden aftershocks? J Struct Geol 26:1109–1125

Cox SF, Knackstedt MA, Braun J (2001) Principles of structural control on permeability and fluid flow in hydrothermal systems. In: Richards JP, Tosdal RM (eds) Structural controls on ore genesis, structural controls on ore genesis. Reviews in economic geology, vol 14. Society of Economic Geologists, Littleton, CO, pp 1–24

Criss RE, Gregory RT, Taylor HP (1987) Kinetic theory of oxygen isotopic exchange between minerals and water. Geochim Cosmochim Acta 51:1099–1108

Daigneault R (1996) Couloirs de déformation de la Sous-Province de l'Abitibi. Ministère des Ressources naturelles du Québec, Québec, p 115

Daigneault R, Mueller WU, Chown EH (2002) Oblique Archean subduction: accretion and exhumation of an oceanic arc during dextral transpression, Southern Volcanic Zone, Abitibi Subprovince Canada. Precambrian Res 115:261–290

Desrochers JP, Hubert C (1996) Structural evolution and early accretion of the Archean Malartic composite block, southern Abitibi greenstone belt, Quebec, Canada. Can J Earth Sci 33:1556–1569

Domenico PA, Schwartz FW (1998) Physical and chemical hydrogeology. Wiley, New York

Eisenlohr BN, Groves DI, Partington GA (1989) Crustal-scale shear zones and their significance to Archean gold mineralization in Western Australia. Miner Depos 24:1–8

Galley AG (1993) Characteristics of semi-conformable alteration zones associated with volcanogenic massive sulphide districts. J Geochem Explor 48:175–200

Garofalo PS (2000) Gold precipitation and hydrothermal alteration during fluid flow through the vein network of the mesothermal gold deposit of Sigma (Abitibi belt, Canada). Swiss Federal Institute of Technology Zurich, Zurich, p 252

Goldfarb RJ, Snee LW, Miller LD, Newberry RJ (1991) Rapid dewatering of the crust deduced from ages of mesothermal gold deposits. Nature 354:296–298

Goldfarb RJ, Groves DI, Gardoll S (2001) Orogenic gold and geologic time: a global synthesis. Ore Geol Rev 18:1–75

Green AG, Milkreit B, Mayrand LJ, Ludden JN, Hubert C, Jackson SL, Sutcliffe RH, West GF, Verpaelst P, Simard A (1990) Deep structure of an Archean greenstone terrane. Nature 344:327–330

Groves DI (1993) The crustal continuum model for the late-Archaean lode-gold deposits of the Yilgarn Block, Western Australia. Miner Depos 28:366–374

Groves DI, Goldfarb RJ, Gebre-Mariam M, Hagemann SG, Robert F (1998) Orogenic gold deposits: a proposed classification in the context of their crustal distribution and relationship to other gold deposit types. Ore Geol Rev 13:7–27

Groves DI, Goldfarb RJ, Robert F, Hart CJR (2003) Gold deposits in metamorphic belts: overview of current understanding, outstanding problems, future research, and exploration significance. Econ Geol 98:1–29

Hagemann SG, Cassidy KF (2000) Archean orogenic lode gold deposits. In: Hagemann SG, Brown PE (eds) Gold in 2000. The Society of Economic Geologists, Littleton, CO, pp 9–68

Hanes JA, Archibald DA, Hodgson CJ, Robert F (1992) Dating of Archeran auriferous quartz vein deposits in the Abitibi Greenstone Belt, Canada: 40Ar/39Ar evidence for a 70- to 100-m.y.-time gap between plutonism–metamorphism and mineralization. Econ Geol 87:1849–1861

Hubert C, Trudel P, Gelinas L (1984) Archean wrench fault tectonics and structural evolution of the Blake River Group, Abitibi Belt, Quebec. Can J Earth Sci 21:1024–1032

Ingebritsen SE, Sanford WE (1998) Groundwater in geologic processes. Cambridge University Press, Cambridge

Irwin PW, Barnes I (1980) Tectonic relations of carbon dioxide discharges and earthquakes. J Geophys Res 85:3115–3121

Jamieson RA, Beaumont C, Fullsack P, Lee B (eds) (1998) Barrovian regional metamorphism: where's the heat? Geological Society, London

Jébrak M, LeQuentrec MF, Mareschal J-C, Blais D (1991) A gravity survey across the Bourlamaque massif, southeastern Abitibi greenstone belt, Québec, Canada: the relationship between the geometry of the tonalite plutons and associated gold mineralization. Precambrian Res 50:261–268

Kerrich R, Ludden J (2000) The role of fluids during formation and evolution of the southern Superior Province lithosphere: an overview. Can J Earth Sci 37:135–164

Kerrich R, Wyman DA (1990) Geodynamic setting of mesothermal gold deposits. An association with accretionary tectonic regimes. Geology 18:882–885

Kerrich R, Fryer BJ, King RW, Willmore LM, van Hees E (1987) Crustal outgassing and LILE enrichment in major lithosphere structures, Archean Abitibi greenstone belt: evidence on the source reservoir from strontium and carbon isotope tracers. Contrib Mineral Petrol 97:156–168

Manning CE, Ingebritsen SE (1999) Permeability of the continental crust: Implications of geothermal data and metamorphic systems. Rev Geophys 37:127–150

Micklethwaite S, Cox SF (2004) Fault-segment rupture, aftershock-zone fluid flow, and mineralization. Geology 32:813–816

Miller LD, Goldfarb RJ, Gehrels GE, Snee LW (1994) Genetic links among fluid cycling, vein formation, regional deformation, and plutonism in the Juneau gold belt, southeastern Alaska. Geology 22:203–206

Muir-Wood R (1994) Earthquakes, strain-cycling and the mobilization of fluids. In: Parnell J (ed) Geofluids: origin, migration and evolution of fluids in sedimentary basins. Geological Society, London, pp 85–98

Neumayr P, Hagemann SG (2002) Hydrothermal fluid evolution within the Cadillac tectonic zone, Abitibi greenstone belt, Canada: relationship to auriferous fluids in adjacent second- and third-order shear zones. Econ Geol 97:1203–1225

Neumayr P, Hagemann SG, Couture J-F (2000) Structural setting, textures, and timing of hydrothermal vein systems in the Val d'Or camp, Abitibi, Canada: implications for the evolution of transcrustal, second- and third-order fault zones and gold mineralization. Can J Earth Sci 37:95–114

Perchuk A, Philippot P, Erdmer P, Fialin M (1999) Rates of thermal equilibration at the onset of subduction deduced from diffusion modeling of eclogitic garnets, Yukon-Tanana terrane, Canada. Geology 27:531–534

Pitre D (2000) Zonation isotopique à l'échelle d'un champ filonien aurifère: le camp mininer de Val-d'Or, Abitibi, Québec Géologie et génie géologique. Université Laval, Québec, p 154

Robert F (1989) Internal structure of the Cadillac tectonic zone southeast of Val d'Or, Abitibi greenstone belt, Quebec. Can J Earth Sci 26:2661–2675

Robert F (1994) Vein fields in gold districts: the example of Val-d'Or, southeastern Abitibi province. Current research part C. Geological Survey of Canada, Ottawa, pp 295–302

Robert F, Brown AC (1986) Archean gold-bearing quartz veins at the Sigma mine, Abitibi greenstone belt, Quebec: part I. Geologic relations and formation of the vein system. Econ Geol 81:578–592

Robert F, Kelly WC (1987) Ore-forming fluids in Archean gold-bearing quartz veins at the Sigma Mine, Abitibi Greenstone belt, Quebec, Canada. Econ Geol 82:1464–1482

Robert F, Boullier A-M, Firdaous K (1995) Gold–quartz veins in metamorphic terranes and their bearing on the role of fluids in faulting. J Geophys Res 100:12861–12879

Roy P, Beaudoin G, Labbé J-Y (1997) Les minéralisations aurifères associées au couloir de déformation de Cameron. Ministère de Ressources Naturelles du Québec, Québec, p 27

Sibson RH, Scott J (1998) Sress/fault controls on the containment and release of overpressured fluids: examples from gold–quartz vein systems in Juneau, Alaska; Victoria, Australia and Otago, New Zealand. Ore Geol Rev 13:293–306

Sibson RH, Robert F, Poulsen KH (1988) High-angle reverse faults, fluid-pressure cycling, and mesothermal gold–quartz deposits. Geology 16:551–555

Tenthorey E, Cox SF (2003) Reaction-enhanced permeability during serpentinite dehydration. Geology 31:921–924

Therrien R, Sudicky EA (1996) Three-dimensional analysis of variably-saturated flow and solute transport in discretely-fractured porous media. J Contam Hydrol 23:1–44

Weinberg RF, Hodkiewicz PF, Groves DI (2004) What controls gold distribution in Archean terranes? Geology 32:545–548

Zoback MD, Townend J (2001) Implications of hydrostatic pore pressures and high crustal strength for the deformation of intraplate lithosphere. Tectonophysics 336:19–30